SEGREGATION OF PARTICLES ON A SANDY RIPPLES BOTTOM CAUSED BY SURFACE WAVES.

Tien-Dat Chu[1] , Armelle Jarno-Druaux[2], François Marin[3], and Alexander Ezersky [4]

Abstract

We report the results of an experimental and theoretical study of the segregation of particles possessing different densities or different dimensions. Sinking particles segregate on sand ripples generated under the action of standing surface waves. It is observed that fine, or light particles may be trapped in a very thin region near the ripple crests. When the surface waves damp, these particles concentrate on the top of ripple crests forming narrow strips, while coarse particles settle more uniformly along the rippled bed. The presented experimental results are explained using simple theoretical model of hydrodynamic flow generated by surface waves near the bottom.

Keywords

Sand ripples, surface waves, segregation.

1. Introduction

Periodic patterns with characteristic spatial period of 5-15 cm is often observed on sea bottom in the coastal zone. These patterns, called sand ripples are very important for the dispersion of pollution, sediment transport and wave damping due to energy dissipation at the bottom. The main part of papers devoted to the formation of pattern on the sea bottom considers sand as homogeneous granular material see, for example [1-3]. However, particles forming seabed are usually heterogeneous. During ripples formation sorting of particles may occur: particles possessing different properties are concentrated in different regions of sand ripples. There exist two types of particles segregation: surface sorting and volume sorting. The number of papers devoted to particles segregation in sand ripples under the action of waves is not very large. Surface sorting is reported in [4–6]: coarse sediments are observed to accumulate mostly along the ripple crests, while fine grains mostly accumulate in the troughs. The presence of fine particles forming very narrow strips on the top of crests is mentioned in [6]. In the case of standing waves, sand bar formation is observed with bar crests composed of coarse sand and flat plateaus of fine sand [7]. The segregation of particles with different densities under the action of highly decaying nonlinear waves is investigated in [8]. Volume segregation was studied in [9, 10]. It was found that segregation of particles with different sizes and densities takes place under the sand ripples in the active bottom layer. The thickness of this layer is approximately of one ripple spatial period. In this layer different patterns like cats eyes [9], sails [10] can appear. Formation of surface segregation patterns and volume patterns may occur simultaneously. The present work aims to study the surface segregation process. We concentrate on particles sorting above a rippled bed under the action of standing waves. Two approaches are compared: we investigate the motion in the ensemble of particles and the motion of individual particles leading to formation of segregation patterns on the bottom surface. Experimental results are explained by theory based on particle motion in viscous fluid.

[1] UMR CNRS 3102 LOMC, University du Havre, 25 rue Philippe Lebon, B .P. 540, 76058 Le Havre Cedex, France. tien-dat.chu@univ-lehavre.fr

[2] UMR CNRS 3102 LOMC, University du Havre, 25 rue Philippe Lebon, B .P. 540, 76058 Le Havre Cedex, France. ajd@univ-lehavre.fr

[3] UMR CNRS 3102 LOMC, University du Havre, 25 rue Philippe Lebon, B .P. 540, 76058 Le Havre Cedex, France.francois.marin@univ-lehavre.fr

[4] UMR CNRS 6143 M2C, University de Caen, 2-4 rue des Tilleuls, Caen 14000, France. Alexander.Ezersky@unicaen.fr

2. Experimental setup and results

2.1 Segregation in the ensemble of particles

The experiments were conducted in two wave flumes (long flume: 9m long and 0.5 m wide; short flume: 5.4 m long, 0.3 m wide). Surface waves are generated by an oscillating paddle at one end of the flume; a near perfect waves reflection takes place at the other end. The heights and the periods of the waves are measured by resistive probes.

The first series of tests was carried out in the long flume with a 20 mm sand layer at the bottom. The water depth h was 0.26 m. Nonlinear waves were excited on the background of a standing wave, and sand ripples were generated on the bottom. The sand is characterized by a median grain diameter d_s = 0.16 mm and by a relative density s=2.65; one volume percent of PVC (polyvinyl chloride) grains with relative density s=1.35 was added to study the particle segregation. For our experiments, we have chosen PVC grains of two types: the first type PVC1 is characterized by a median grain diameter d_1=0.12 mm, while the second type PVC2 has a median grain diameter d_2=0.20 mm. Experimental conditions may be characterized by the two following non-dimensional parameters: the Froude number (Fr), and the Stokes number (St) number:

$$Fr = U_b / \sqrt{((\rho_{S,PVC} / \rho_w) - 1) g d_{s,PVC}} \quad , \quad St = d^2_{s,PVC} \rho_{s,PVC} \omega / 18 \nu \rho_w \qquad (1),$$

where U_b is the amplitude of the flow velocity close to the bottom, ρ is the density, ω the flow pulsation, v the fluid kinematic viscosity, and the indices s, PVC, and w correspond to sand, PVC, and water, respectively. The value of Fr may be estimated to be 8 for the sand, 20 for the PVC1 grains, and

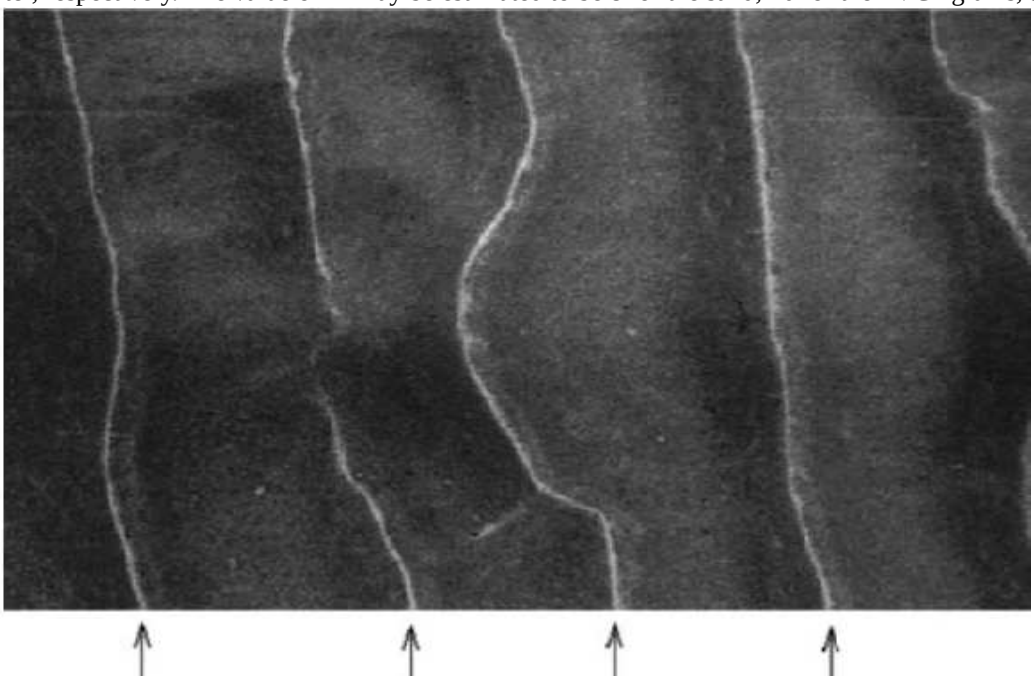

Figure 1 Typical top view of the concentration of PVC grains on the ripple crests marked by arrows.

15 for the PVC2 grains. The Stokes number is a small parameter for the present tests: we have $St=4\,10^{-3}$ for the sand, $St=10^{-3}$ for the PVC1 grains, and $St=3\,10^{-3}$ for the PVC2 grains.

The experiments were carried out as follows. Before each test, the sand and the plastic PVC1 or PVC2 grains were carefully mixed and the mixture was distributed uniformly over the bottom of the flume; the bed was initially flat for all the tests. Because of the small concentration of plastic grains they could hardly be seen on the bottom. We switched on the wave maker and a steady-state regime of non linear wave excitation was obtained after a few minutes. Ripples formed rapidly along the flume and a strong interaction occurred between the bed ripples and the nonlinear surface waves, as shown in [11].

Because of large intensity of surface wave, turbulence in the vicinity of the bottom was generated and some part of particles was suspended over the rippled bottom. It should be noted that the size and the shape of ripples significantly change from one end of the flume to the other end, in the same way as for homogeneous sediments [11]. The wave maker was switched off when the steady state of the surface wave—bed ripple system was reached. At this steady state, the characteristic ripple wavelength and height were 15 and 2.5 cm, respectively, in the area where the ripples were the biggest, that is, close to the nodes of the standing harmonic wave located at one quarter and three-quarters of the flume length [12]. A short time later, the wave motions in the channel were damped; the characteristic time of surface wave decay was T_d=1/ 300 s. As the wave motions were damping, suspended particles sink and we observed the appearance of regions where PVC grains accumulated. The grains were concentrated in a narrow region in the immediate vicinity of ripple crests (Fig. 1). Despite the small concentration of plastic grains in the PVC1-sand and PVC2-sand mixtures, this effect was excellently visualized because of the different colors of PVC and sand.

2.2 Individual motion of particles

The second series of experiments was carried out in the short flume. Before the investigation of particle segregation, ripples on the bottom were generated. For this purpose the frequency of the oscillating paddle is chosen close to the resonant frequency f_r = 0.31 Hz of the mode whose wavelength is equal to the effective flume length (L_w = 5 m). The water depth at rest h is 0.26 m. Only a standing wave was generated for the second series of experiments; no non linear waves was excited contrary to the first series of experiments. For the present tests, the maximum wave height at the antinode H is 0.04 m. Ripples were generated beneath standing waves from the initially flat bed, which consisted in a 4-cm layer of polyvinyl chloride (PVC2). Ripples formed rapidly along the flume once the wave maker was switched on. Their size and shape change from one end of the flume to the other end, depending on their position in relation to the position of the nodes and antinodes of the standing wave. The regions under the antinodes are essentially flat, whereas the regions under the nodes where the bed shear stress is maximum are covered by the greatest ripples.

When the equilibrium state is reached, we switch off the oscillating paddle and empty slowly the wave flume in order to maintain the natural form of the bed. The rippled bed is then covered by a thin powdering of cement. When this powdering is dry, the wave flume is refilled with the same water level at rest as previously (0.26 m). PVC particles are then carefully injected through the free surface above the fixed rippled bed, and their trajectories are registered. The studied zone for the particle trajectories and the sediment sorting is chosen close to the node located in the vicinity of the wall reflecting the surface waves. In this zone, ripples are mostly regular and bidimensional; their wavelength L_r and their height H_r are, respectively, 5.5 cm and 1.5 cm.

Grain trajectories were obtained performing particle tracking velocimetry (PTV). In the experiments five different kinds of PVC particle (0.11, 0.19, 0,28, 0.45 and 0.57 mm in diameter) have been used. The principle of PTV is to individually follow each introduced particle in successive images. A high-

resolution camera Dalsa Falcon PT-41-4M60 (resolution 2352 × 1728 pixels), 62 frames per second, is used in combination with a laser diode, which generates a thick vertical light sheet. The thickness of the light sheet is fixed to two centimeters so that particles stay long enough in the illuminated area to enable the capture of grain trajectories over several wave periods [13,14].
Particle trajectories are obtained using a program presented in Ref. [15] and adapted to the present experiments. For present tests, two phases of the flow were considered: during the excitation of standing waves [phase (1)] and during the decay of surface waves [phase (2)], after the stopping of the oscillating paddle.

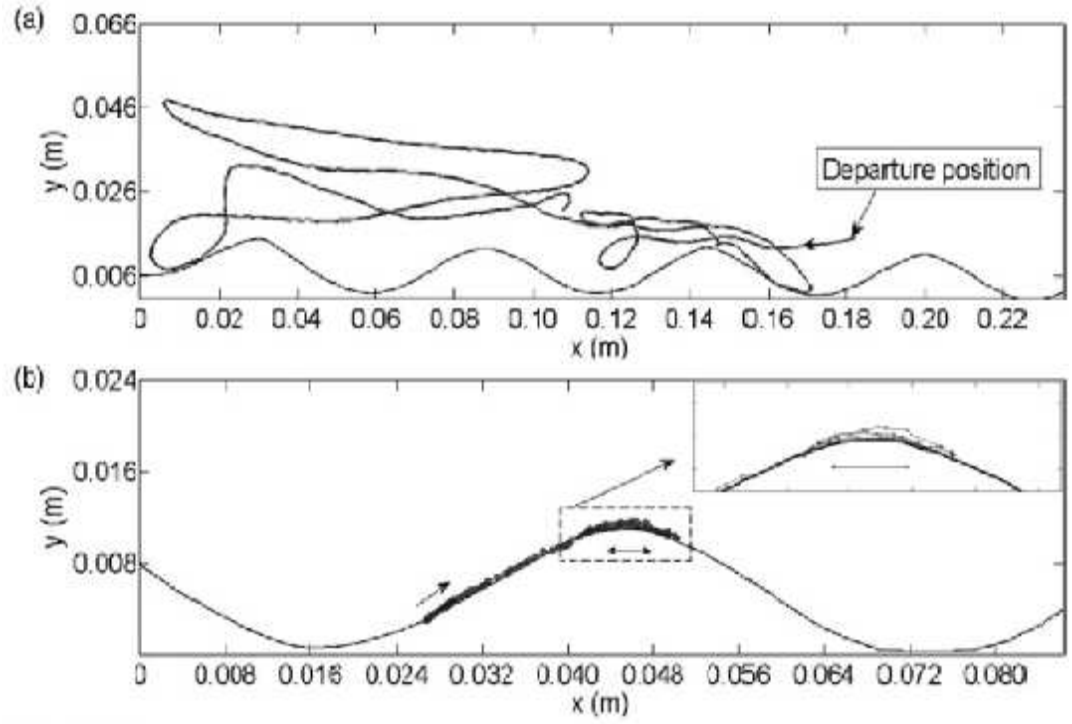

Figure 2. Typical particle trajectory.

The motion of particles near the bottom is caused by organized vortices which are forming on the lee side of ripples and shed above ripple crests each half-cycle [16,17]. Figure 2(a) depicts a typical trajectory above the rippled bed under the effect of vortices showing the complex motion of particles. Let us focus on the area close to ripple crests. The oscillating movement of particles in a zone confined just above the top of the ripple crests can be observed, as shown in Fig. 2(b). In this confinement zone, particles can be "captured" and ejected in the flow several periods later. Form and dimensions of the confined zone are determined by the extreme positions of grains that oscillate in it. Its lower limit is the ripple crest and its height varies from zero at its extremities to H_{cz} = 0.9 mm at the top of the ripple crest; this height is comparable with the Stokes layer thickness, $\delta = (2\nu/\omega)^{1/2} \approx 1$ mm, and is greater than the grain size. The length L_{cz} of the confinement zone may be estimated at 10.9 mm, which corresponds approximately to one-fifth of the ripple wavelength in the tested zone. Present tests show that the ejected particles are the ones for which the diameter d_p is greater than approximately 0.28 mm. These particles are more exposed to the vortices than finer ones. We measured the mean resident time of particles in the confinement zone according to the sediment size. This time varies from one-half to two or three times the wave period for coarse particles. It is much

longer for very fine and fine particles, ranging from three times the wave period to the total duration of the experiment. The grains capture and ejection at ripple crests may be considered as a sediment sorting process.

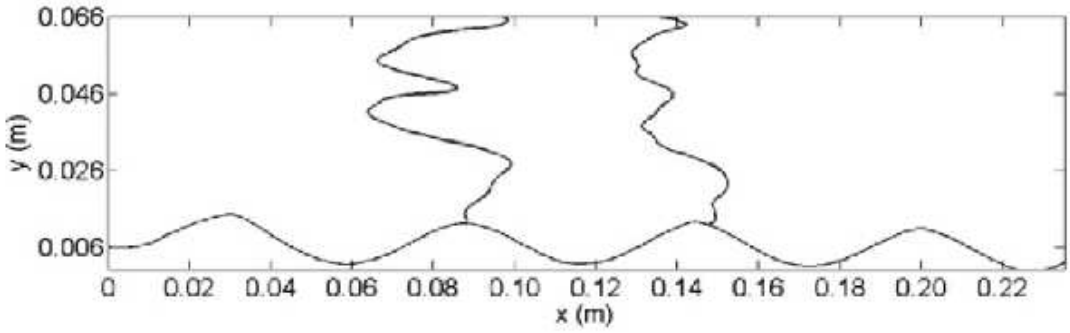

Figure 3 Typical particle trajectories during the waves damping.

When the oscillating paddle is stopped, suspended particles start to settle under the action of gravity. The settling velocity of the coarse particles (d_p = 0.45 mm) is about 15 times larger than the one for the very fine particles (d_p = 0.11 mm). As shown in Fig. 3, the amplitude of motion of coarse particles before they reach the bed is large, since these particles begin to settle rapidly after a few wave periods ($t \approx$ 2–3 T) when the hydrodynamic forcing is still intense. Coarse particles generally reach the bed after a trajectory composed of four lateral excursions in the observation window.

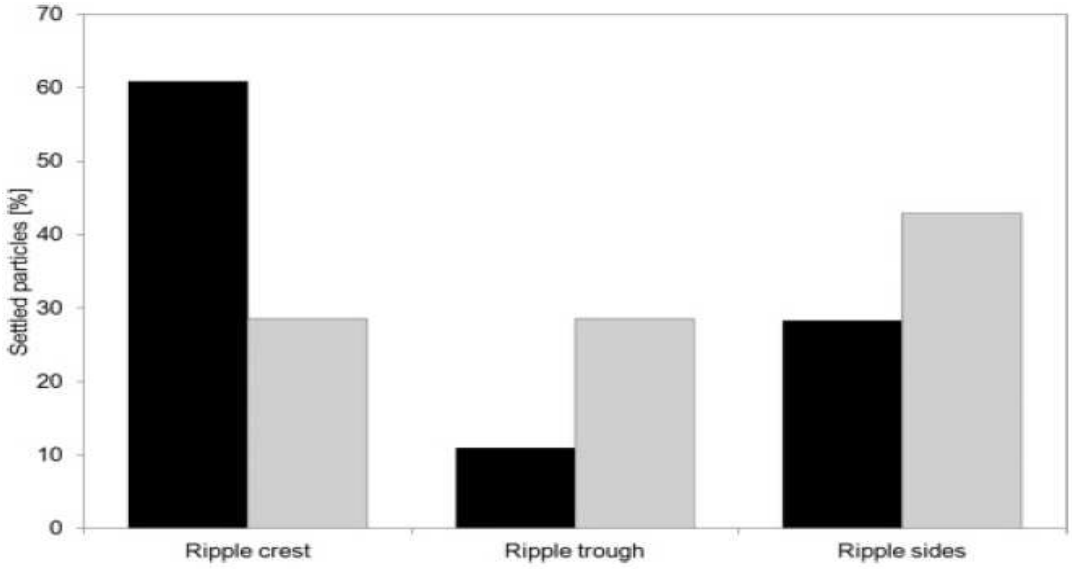

Figure 4. Distribution of settled particles along the rippled bed surface. Black column: d_p =0.11mm, 0.19 mm, 0.28 mm, gray column d_p =0.45 mm, d_p =0.57 mm

On the other hand, finer particles, which are lighter, reach the bed later when the amplitude of fluid motion is weaker; the number of lateral excursions increases when particle size decreases. The maximum number of lateral excursions is equal to 10 for very fine particles (d_p = 0.11 mm). About 100 trajectories of sinking particles have been measured. The initial positions of these particles at the

upper limit of the observation window are horizontally uniformly distributed above ripples. Places where the grains settle along the rippled bed are analyzed according to their size. The histogram of repartition of particles deposition zone over the three regions delimiting the ripple crest, trough, and both sides is shown in Fig. 4. The length of the region defining the vicinity of ripple crest is fixed to 10 mm (18 % of the ripple wavelength in the considered zone) divided equally on both sides of the top of the ripple. The length of the trough region is estimated at 16 mm; both sides occupy 29 mm. The results show that 61 % of the very fine and medium particles settle in the vicinity of the ripple crests, whereas 39 % of these particles settle elsewhere. In the case of coarse particles, only 29 % of grains settle in the vicinity of the crests. Furthermore, for the range of coarse particles considered herein, no privileged deposition place is noted.

The concentrations of suspended particles have been obtained in a 1-cm-high horizontal strip. Its lowest level is 2.9 mm above the highest point of the bed. In this strip, zones delimiting regions above ripple crests are 10mm long when regions above ripple troughs are 16 mm long. Particle concentrations per unit area have been obtained in the following way: the number of particles crossing the strip is counted during their settling when the water waves damp. The strip is in a vertical plane illuminated by a laser diode.

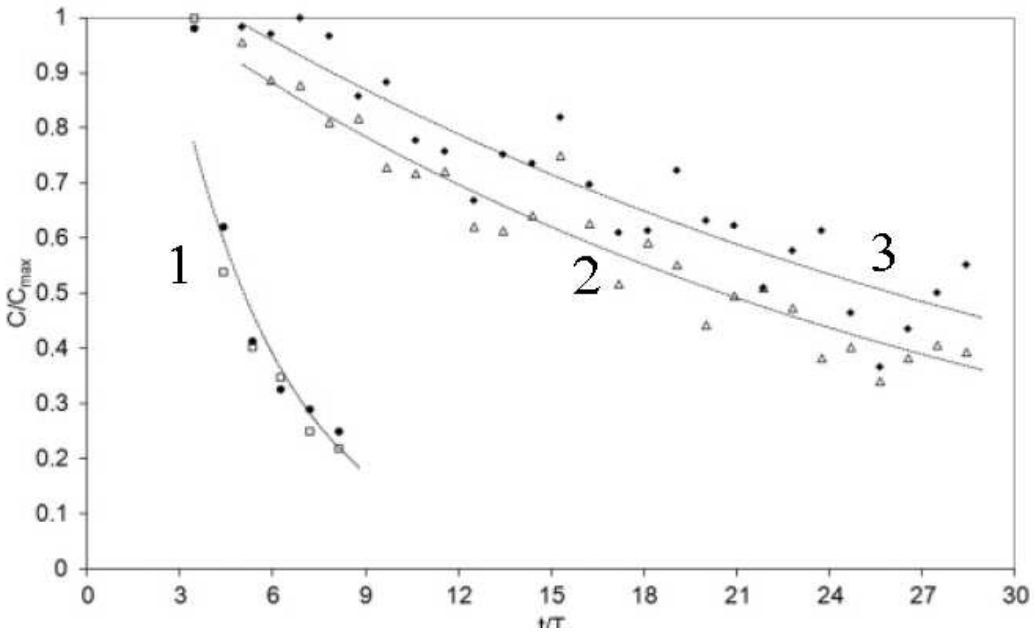

Figure 5 Temporal evolution of particle concentrations close to the bottom when surface waves damp: curve 1 d=0.45 mm and d=0.57 mm above ripple crest and trough; curve 2 d_p =0.11 mm, d_p =0.19 mm and 0.28 mm above ripple trough; curve 3 d_p =0.11 mm, d_p =0.19 mm and 0.28 mm above ripple crest.

The particles concentration C is estimated along the strip as $C = n/S$, where n is the number of detected particles in the considered zone and S is the surface of this zone. The temporal evolution of relative concentration C/C_{max} is shown in Fig. 5, where C_{max} is the maximum concentration measured over all the experiments during the settling process. The origin of the temporal axis $t = 0$ corresponds to the time when the oscillating paddle is stopped. This figure exhibits an exponential decrease of C/C_{max} with t/T . The particles with d_p = 0.45 mm and d_p =0.57 mm (curve 1, Figure 5) settle rapidly and regularly without significant difference between the concentrations above the ripple crests and troughs. As far as the particles with sizes d_p =0.11 mm, d_p =0.19 mm and d_p =0.28 mm are concerned,

the two plotted curves (curves 2,3 Figure 5) exhibit similar variations and a trend to higher concentration above the crests that can be interpreted as a size sorting above the rippled bed during the particle settling when the surface waves damp. The concentration distributions show temporal fluctuations of fine grains when these distributions are more regular for coarser grains. These are the result of the high sensitivity of the light particles to the fluid movement until the water becomes totally still.
The changes in light particle concentration on the rippled bed and the investigation of trajectories of small and large particles demonstrate that there exists a mechanism of particle sorting under the action of surface waves due to the bottom profile. A theoretical description of such kind of sorting is considered in the next paragraph.

3. Theoretical approach.

We consider a very simple model for the flow in a narrow region near the ripple crests neglecting in the first approximation the curvature of the crests. Using experimental data we model this flow in the neighborhood of each sand crest by the stream function:

$$U_x = \frac{\partial \psi}{\partial y} = -a\left[\alpha\left(x + x_0\right) + 2y\right], \qquad U_y = -\frac{\partial \psi}{\partial x} = a\alpha y. \quad (2)$$

The point $x=0, y=0$ corresponds to the ripple crest. Streamlines of this flow are shown in Fig.6.

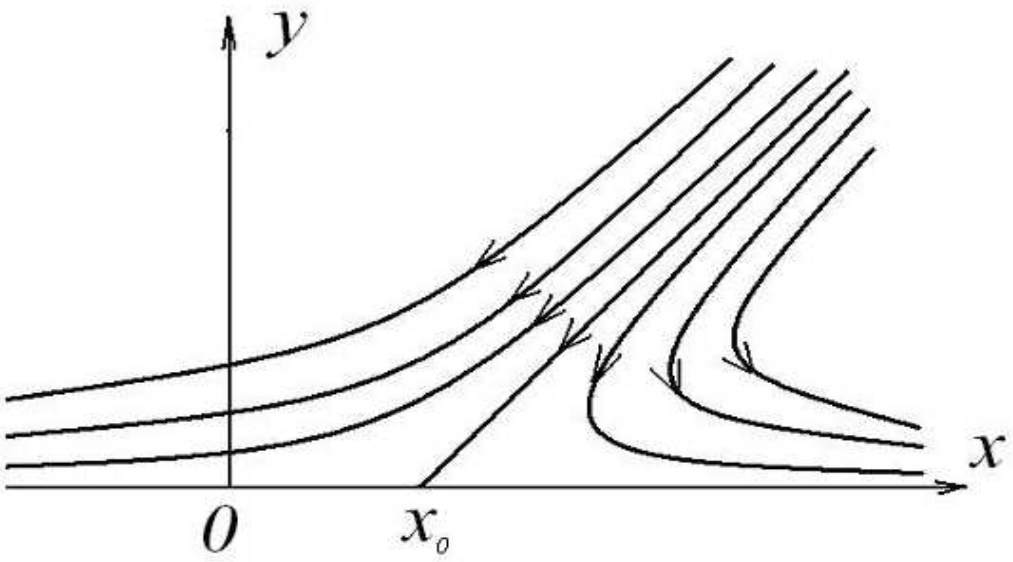

Figure 6. Theoretical model of flow near ripple crest.

The point $x=x_0, y=0$ is so called hyperbolic point.
In our model, the coefficient $\alpha=\alpha_0 sin(\omega t)$ is the parameter that controls the slope of the line separating the forward and return flows. The value of α_0 may be estimated from flow visualization: α_0 ~ 1rad. The coefficient $a=a_0 sin(\omega t)$ is related to the vorticity $\Omega = 2a\vec{z}$, where $\vec{z}$ is a unit vector

perpendicular to the flow plane. A slip condition is assumed on the surface y=0. We suppose that the thickness of the oscillating boundary layer $\delta \approx 1$ mm is much less than the other characteristic scales of motion in the vicinity of the ripple crest.

A particularity of our model is the presence of an oscillating movement of the hyperbolic point: $x_0=X_0 sin(\omega t)$, where X_0 is the amplitude of displacement of hyperbolic point relative to the ripple crest.

The particle velocity V does not coincide with the flow velocity U. For our experimental conditions, the Stokes number is a small parameter ($St \sim 10^{-3}$, 10^{-2}) that we use as an expansion parameter. The particle velocity is written as

$$\vec{V} = \vec{V}^{(0)} + St\vec{V}^{(1)} + St^2\vec{V}^{(2)} + \ldots \tag{3}$$

Neglecting all terms proportional to St^2 in Eq. (3), the particle velocity field may be written as follows [18]:

$$V_x = U_x - \frac{St}{\omega}\sigma\frac{dU_x}{dt}, \tag{4}$$

$$V_y = U_y - U_0 - \frac{St}{\omega}\sigma\frac{dU_y}{dt}, \tag{5}$$

where V_x and V_y are the projections of the particle velocity vector onto the horizontal and vertical directions, and $\sigma=1-\rho_w/\rho_{s,PVC}$. After the substitution of Eqs. (2) into Eqs. (4) and (5), we obtain the following expressions for the particle velocities close to the ripple crests:

$$V_x = -a\left[\alpha\left(x+x_0\right)+2y\right] + \frac{St}{\omega}\sigma\left[\left(\dot{a}\alpha + a\dot{\alpha}\right)\left(x+x_0\right) + 2\dot{a}y - a^2\alpha^2\left(x+x_0\right) + a\alpha\dot{x}_0\right], \tag{6}$$

$$V_y = a\alpha y - U_0 - \frac{St}{\omega}\sigma[\left(\dot{a}\alpha + a\dot{\alpha}\right)y + a^2\alpha^2 y]. \tag{7}$$

It is supposed that after the oscillating paddle is stopped, the turbulence decays much more rapidly than the waves. During the wave damping, it is reasonable to consider that the vorticity and the length of the confinement zone decay in the same way as the amplitude of the surface waves. We suppose that the change of the amplitude of particles velocity during a wave period is small compared with the particles velocity amplitude. The particles velocity temporally averaged over a wave period $T=2\pi/\omega$ is easily obtained from Eqs. (6) and (7):

$$\left\langle V_x \right\rangle = -a_0\alpha_0 e^{-\gamma t}\left[\frac{1}{2} + \frac{St}{\omega}\sigma\left(\gamma + \frac{3}{8}a_0\alpha_0 e^{-\gamma t}\right)\right]x \tag{8}$$

$$\left\langle V_y \right\rangle = a_0\alpha_0 e^{-\gamma t}\left[\frac{1}{2} + \frac{St}{\omega}\sigma\left(\gamma - \frac{3}{8}a_0\alpha_0 e^{-\gamma t}\right)\right]y - U_g \tag{9}$$

where γ is the rate of exponential decay of surface waves and U_g is the velocity of sinking of

particles:

$$U_g = \frac{2gd_2(\rho_p - \rho_w)}{18\nu\rho_w} \quad . \tag{10}$$

The horizontal component $<V_x>$ is negative for $x > 0$ and positive for $x < 0$, and particles tend to move toward the ripple crest ($x = 0$) when the surface waves damp. The rate of exponential decay for the present surface waves is estimated at $\gamma = 0.021$ s^{-1} from measurements of the temporal evolution of surface waves using resistive probes. Figure 7 shows typical particle trajectories for different initial positions and two median diameters: $d_p = 0.45$ mm and $d_p = 0.28$ mm. The fine particles ($0.11 \le d_p \le 0.28$ mm) are found to settle close to ripple crests when the coarser ones may fall everywhere on the bed. These particles settle on the bottom after only a few wave periods; Figure 5 exhibits that most of them reach the area very close to the bottom approximately for $4 \le t/T \le 9$, when the damping time of surface waves is much greater ($1/\gamma \approx 48$ s $\approx 15T$). For $d_p \le 0.28$ mm, the time for particles to reach the bottom is greater; Figure 5 shows that when $t/T = 30$, particles are not all deposited on the bed. The settling area near the ripple crests is well predicted by the present theoretical model.

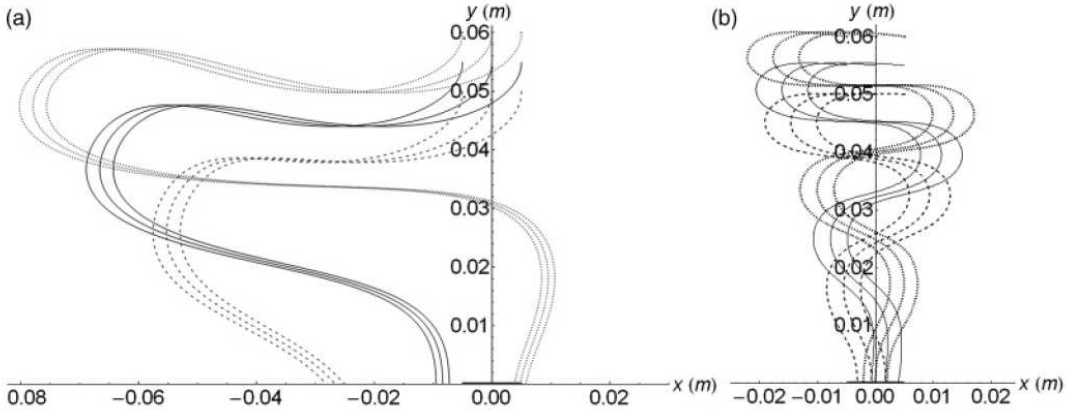

Figure 7. Theoretical trajectories starting from nine different initial points above the ripple crest: a) $d_p = 0.45$ mm, b) $d_p = 0.28$ mm.

We are able to predict changes in concentration of particles caused by averaged flows. Using the conservation law for particles concentration we get:

$$\frac{\partial C}{\partial t} + \nabla(C\langle\vec{V}\rangle) = 0 \quad , \quad \langle\vec{V}\rangle = \left(\langle V_x\rangle, \langle V_y\rangle\right) \tag{11}$$

Supposing spatially homogeneous changes of concentration C_{crest} in the vicinity of the hyperbolic point, we have the following evolution equation for C_{crest}:

$$\boxed{\frac{\partial C_{crest}}{\partial t} = \frac{3}{4}\sigma\frac{St}{\omega}C_{crest}a_0^2\alpha_0^2\exp(-2\gamma t)} \tag{12}$$

The concentration of particles grows with time and for full decaying of waves, the relative changes of concentration is:

$$\frac{\delta C_{crest}}{C_{crest,0}} = \frac{3}{8}\sigma \frac{St}{\gamma\omega} a_0^2 \alpha_0^2 \qquad (13)$$

Our simple model shows that the grain concentration grows in the vicinity of the hyperbolic point with increasing values of the time. Using this result it is possible to understand why sorting of particles occurs in experiments with mixture of sand and PVC described in section 2.1. The characteristic time of this process equals the time of surface wave decay, $T_d=1/\gamma$. It should be emphasized that the increase of the concentration of sand and PVC grains occurs in different ways. Indeed, let us estimate the sedimentation times. Due to turbulence the grains were suspended in a layer approximately D_l~20 cm thick. The time necessary for the suspended grains to reach the bottom after the wave maker was stopped may be estimated to be $\tau_s \sim D_1 / U_{0s}$=9s for the sand, τ_{PVC1} ~70 s for the PVC1 grains, and τ_{PVC2} ~30 s for the PVC2 grains. The concentration of the PVC grains should consequently increase everywhere at the bed surface; however, the PVC grains are observed only close to the ripple crests when the waves have damped. The segregation mechanism may be explained as follows. After the wave maker has been stopped and for $t<\tau_s$, both sand and PVC grains are concentrated near the ripple crests. For $t>\tau_s$, when most sand grains have settled on the bottom, only PVC grains begin to concentrate near the crests. It is possible to estimate the increase in PVC grain concentration using Eq. (13) with $t=\tau_{PVC1,2}$. For the present experimental conditions, we get: $\langle C\rangle / \langle C_0\rangle$ ~ 20 for the PVC1 grains and $\langle C\rangle / \langle C_0\rangle$ ~ 50 for PVC2 grains. This explains why the PVC grains, characterized by a lower density than that for the sand grains, concentrate close to the ripple crests, at the end of the surface wave decay.

4. Conclusions

This paper presents an experimental and theoretical study of particle size and density sorting above sand ripples appearing as a result of instability under the action of water waves. Laboratory experiments revealed different types of particle segregation on the bottom. Light particles and particles with small dimension concentrate in the vicinity of ripple crest. Such segregation effect may be very important in natural conditions for different biological problems and environment processes. For example, this segregation can be responsible for anomalous increasing of concentration of pollution and microorganisms in the vicinity of ripple crest on the sea bottom.

References

[1] P.Blondeaux. Sand ripples under sea waves. Part 1. Ripples formation. *J.Fluid Mech*. 1990, v.218, p.1-17.
[2] G.Vittori, P.Blondeuax. Sand ripples under sea waves. Part 2. Finite amplitude-development. *J.Fluid Mech.* 1990, v.218, p.19-39.
[3] J. Lebunetel-Levaslot, A. Jarno-Druaux, A.B. Ezersky, F. Marin, Dynamics of propagating front into sand ripples under regular waves, *Phys.Rev E,* 2010, v.82, 032301.
[4] E. Foti and P. Blondeaux, Sea ripple formation: The heterogeneous sediment case. Coastal Eng. **25**, 237 (1995).
[5] J. S. Doucette, Geometry and grain-size sorting of ripples on low-energy sandy beaches: field observations and model predictions ; Sedimentology **49**, 483 (2002).

[6] S. Balasubramanian, S. I. Voropayev, and H. J. S. Fernando, Grain Sorting and Decay of Sand Ripples Under Oscillatory Flow and Turbulence; J.Turbulence **9**, 1 (2008).
[7] B. J. Landry, M. J. Hancock, and C. C. Mei, Note on sediment sorting in a sandy bed under standing water waves. Coastal Eng. **54**, 694 (2007).
[8] A. B. Ezersky and F. Marin, Segregation of sedimenting grains of different densities in an oscillating velocity field of strongly nonlinear surface waves; Phys. Rev. E **78**, 022301 (2008).
[9] G.Rousseaux, H.Caps, J.-E.Wesfreid, Granular size segregation in underwater sand ripples, Eur. Phys. J. E 2004, 13, 213-219.
[10] T. D. Chu Dynamique sédimentaire en zone côtière dans le cas de sédiments multi-classes Thèse, Le Havre 2012.
[11] F. Marin, N. Abcha, J. Brossard, and A. B. Ezersky, Laboratory study of sand bed forms induced by solitary waves in shallow water, J. Geophys. Res. **110**, F04S17 2005.
[12] A. Ezersky, O. Poloukhina, J. Brossard, F. Marin, and I. Mutabazi, Spatio-temporal properties of solitons excited on the surface of shallow water in a hydrodynamic resonator, Phys. Fluids **18**, 067104 2006.
[13] F. Hering, C. Leue, D.Wierzimok, and B. Jähne, Particle tracking velocimetry beneath water waves. Part I: visualization and tracking algorithms, Exp. Fluids **23**, 472 (1997).
[14] F. Hering, C. Leue, D.Wierzimok, and B. Jähne, Particle tracking velocimetry beneath water waves part II: Water waves, Exp. Fluids **24**, 10 (1998).
[15] S. S. Rogers, T. A. Waigh, X. Zhao, and J. R. Lu, Precise particle tracking against a complicated background: polynomial fitting with Gaussian weight, Phys. Biol. **4**, 220 (2007).
[16]F. Marin, Eddy viscosity and Eulerian drift over rippled beds in waves. Coastal Eng. **50**, 139 (2004).
[17] J. J. Van der Werf, V. Magar, J. Malarkey, K. Guizien, and T. O'Donoghue, 2DHV modelling of sand transport processes over full-scales ripples in regular oscillatory flow. Cont. Shelf Res. **28**, 1040 (2008).
[18] T.D. Chu, A. Jarno-Druaux, F. Marin, A.B. Ezersky, Particle trajectories and size sorting above a rippled bed under standing water waves, Physical Review E **85**, 2 (2012).